Confinement of β_1- and β_2-adrenergic receptors in the plasma membrane of cardiomyocyte-like H9c2 cells is mediated by selective interactions with PDZ domain and A-kinase anchoring proteins but not caveolae

Cathleen D. Valentine and Peter M. Haggie
Division of Nephrology, Department of Medicine, University of California, San Francisco, San Francisco, CA 94143

ABSTRACT **The sympathetic nervous system regulates cardiac output by activating adrenergic receptors (ARs) in cardiac myocytes. The predominant cardiac ARs, β_1- and β_2AR, are structurally similar but mediate distinct signaling responses. Scaffold protein–mediated compartmentalization of ARs into discrete, multiprotein complexes has been proposed to dictate differential signaling responses. To test the hypothesis that βARs integrate into complexes in live cells, we measured receptor diffusion and interactions by single-particle tracking. Unstimulated β_1- and β_2AR were highly confined in the membrane of H9c2 cardiomyocyte-like cells, indicating that receptors are tethered and presumably integrated into protein complexes. Selective disruption of interactions with postsynaptic density protein 95/disks large/zonula occludens-1 (PDZ)–domain proteins and A-kinase anchoring proteins (AKAPs) increased receptor diffusion, indicating that these scaffold proteins participate in receptor confinement. In contrast, modulation of interactions between the putative scaffold caveolae and β_2AR did not alter receptor dynamics, suggesting that these membrane domains are not involved in β_2AR confinement. For both β_1- and β_2AR, the receptor carboxy-terminus was uniquely responsible for scaffold interactions. Our data formally demonstrate that distinct and stable protein complexes containing β_1- or β_2AR are formed in the plasma membrane of cardiomyocyte-like cells and that selective PDZ and AKAP interactions are responsible for the integration of receptors into complexes.**

Monitoring Editor
Robert G. Parton
University of Queensland

Received: Jan 13, 2011
Revised: May 31, 2011
Accepted: Jun 7, 2011

INTRODUCTION

G-protein–coupled receptors (GPCRs) constitute the largest family of membrane-bound receptors, initiate diverse signal processes, and are the targets for many drugs (Pierce *et al.*, 2002; Lagerström and Schiöth, 2009). In the heart, GPCRs in the adrenergic receptor (AR) family bind catecholamines to convert sympathetic nervous system stimulation into cardiovascular responses. Cardiac myocytes express nine ARs; however, the β_1- and β_2AR subtypes have been demonstrated to largely regulate contractile function (Xiang and Kobilka, 2003; Xiao *et al.*, 2006). Although structurally very similar, β_1- and β_2AR initiate different signaling cascades and undergo different trafficking processes in cardiac myocytes (Rockman *et al.*, 2002; Xiang and Kobilka, 2003; Xiao *et al.*, 2006). For instance, β_1AR stimulation is manifest by an increase in contraction rate, whereas β_2AR activation produces a biphasic response, with an initial increase followed by a sustained decrease in contraction rate (Xiang and Kobilka, 2003; Xiao *et al.*, 2006). Activated β_1AR is retained at the cell surface, whereas activated β_2AR is internalized to mediate desensitization (Xiang *et al.*, 2002a; Xiang and Kobilka, 2003). Furthermore, chronic stimulation of β_1AR is proapoptotic, whereas

This article was published online ahead of print in MBoC in Press (http://www.molbiolcell.org/cgi/doi/10.1091/mbc.E11-01-0034) on June 16, 2011.

Address correspondence to: Peter M. Haggie (peter.haggie@ucsf.edu).

Abbreviations used: AKAP, A-kinase anchoring protein; AR, adrenergic receptor; CFTR, cystic fibrosis transmembrane conductance regulator; PDZ, postsynaptic density protein 95/disks large/zonula occludens-1; Qdots, quantum dots; SPT, single-particle tracking.

persistent β_2AR activation is cardioprotective (Zheng *et al.*, 2005; Xiao *et al.*, 2006).

Compartmentalization of βARs in plasma membrane microdomains containing specific proteins with scaffolding and catalytic activities has been proposed to explain subtype-specific cardiac adrenergic signaling (Hall and Lefkowitz, 2002; Xiang and Kobilka, 2003; Malbon *et al.*, 2004; Steinberg, 2004; Xiao *et al.*, 2006). Scaffold proteins associate with two or more proteins to increase the efficiency or specificity of a signaling pathway and usually contain at least one protein–protein interaction domain (Wong and Scott, 2004; Zeke *et al.*, 2009). In various cell types, association between β_2AR and scaffolds, including caveolin-3 (CAV3), A-kinase anchoring protein 5 (AKAP5; alternative names human AKAP79 and murine AKAP150), AKAP12 (human gravin/AKAP250 or murine SSeCKS), and postsynaptic density protein 95/disks large/zonula occludens-1 (PDZ)–domain proteins, including ezrin-binding phosphoprotein of 50 kDa (EBP50; alternative names NHERF1 or Slc9a3r1), have been demonstrated by biochemical and functional assays (Hall *et al.*, 1998a, 1998b; Fraser *et al.*, 2000; Rybin *et al.*, 2000; Fan *et al.*, 2001; Xiang *et al.*, 2002b; Tao *et al.*, 2003; Balijepalli *et al.*, 2006). Similarly, functional and biochemical assays have demonstrated association between β_1AR and AKAP5 and PDZ domain proteins, including synapse-associated protein of 97 kDa (SAP97; alternative name Dlg1) and postsynaptic density protein 95 (PSD-95) (Gardner *et al.*, 2006; He *et al.*, 2006). In addition, interaction with the cytoskeleton may influence receptor compartmentalization, as many putative receptor scaffolds, including PDZ-domain proteins, AKAPs, and caveolae, interact directly or indirectly with the actin cytoskeleton (Wu *et al.*, 1998; Bretscher *et al.*, 2000; Gomez *et al.*, 2002; Pelkmans and Zerial, 2005).

Understanding the physical nature of adrenergic receptor complexes has important implications on a basic level and for the design of therapeutic approaches for cardiomyopathies (Negro *et al.*, 2008). Although a large body of data supports the concept of compartmentalized signaling in cardiac myocytes, no information is available to describe receptor dynamics in the plasma membrane of cardiac myocytes or the contribution of potential scaffolds to complex integrity and stability. In addition, studies that support the concept that receptors are compartmentalized are not without caveats. For instance, biochemical approaches that demonstrate protein interactions generally provide no information regarding the degree or dynamics of protein association and are typically performed in dilute, nonphysiological solutions. Similarly, studies that implicate caveolae in receptor scaffolding often use pharmacological maneuvers that alter many cellular processes (Hancock, 2006). In this study, single-particle tracking (SPT) was applied to test the hypothesis that βARs integrate into stable, discrete protein complexes in live cardiomyocyte-like H9c2 cells. The involvement of PDZ-domain proteins, AKAPs, caveolae, and actin in receptor dynamics was systematically investigated using maneuvers that modulated interactions between these scaffolds and receptors.

RESULTS

β_1AR and β_2AR are confined in the plasma membrane of H9c2 cells

The diffusion and interactions of unstimulated β_1- and β_2ARs were studied in H9c2 cardiomyocyte-like cells by SPT of engineered receptors containing amino-terminal hemagglutinin (HA) tags. These receptor analogues recapitulate the signaling and trafficking properties of untagged receptors in a variety of cell systems, including cardiac myocytes (Cao *et al.*, 1999; Luttrell *et al.*, 1999; Xiang *et al.*, 2002a; Shcherbakova *et al.*, 2007). H9c2 cells express endogenous β_1- and β_2AR, and transfection conditions were initially established such that overexpression of epitope-tagged receptors did not result in substantially increased levels of either receptor. In HA-β_1AR–transfected cells, the total levels of β_1AR (β_1AR plus HA-β_1AR) increased only ~1.5-fold, and similar increases in β_2AR levels were observed in HA-β_2AR–transfected cells (levels were characterized by quantitative immunohistochemistry, as described in *Materials and Methods*). Using these transfection conditions, HA-tagged adrenergic receptors expressed in H9c2 cells demonstrate similar properties as in neonatal cardiac myocytes; for instance, HA-β_1AR was retained at the cell surface upon isoproterenol stimulation, whereas HA-β_2AR was internalized (Supplemental Figure S1; Xiang *et al.*, 2002a). For SPT, epitope-tagged receptors were labeled by successive incubation of transfected cells with anti-HA antibody, biotin-conjugated Fab fragments, and streptavidin conjugated, 655 nm emitting quantum dots (Qdots). Qdot attachment was selective such that individual fluorophores with intermittent emissions could be observed on the surface of HA-β_1– or HA-β_2AR–expressing cells, whereas neighboring, untransfected cells showed near-zero nonspecific labeling (Supplemental Figure S2).

To characterize the diffusive properties of Qdot-labeled receptors, image sequences were acquired at 30 frames per second (fps) over 20 s. Figure 1A shows frames from representative image sequences for Qdot-labeled HA-β_1AR (top) and HA-β_2AR (bottom) (see Supplemental Movies S1 and S2; note that intermittent fluorescent emissions confirm that individual Qdots were imaged). Visual inspection of image sequences indicated that both receptors were confined over the data acquisition period. Time-lapse imaging acquired at 1 fps qualitatively confirmed that receptor confinement persisted over a time scale of minutes (Figure 1B). To quantify receptor diffusion, individual trajectories were reconstructed from SPT image sequences. As expected, trajectories for HA-β_1AR (Figure 1C, left) and HA-β_2AR (Figure 1C, right) were highly confined, typically being restricted to membrane domains of approximately 200 nm diameter. Trajectories derived from Qdot-labeled receptors in live cells were more mobile than those derived from fixed cells or from Qdots immobilized on a glass surface (Figure 1C, bottom) indicating that trajectories in live cells, albeit highly confined, report actual receptor diffusion. Individual trajectories were analyzed to generate mean-squared displacement (MSD) versus time plots, and values of short-range diffusion coefficient (D) and range ($MSD^{1/2}$, a representation of how far receptors move in 2 s) determined (Haggie *et al.*, 2006; Crane and Verkman, 2008). Figure 1D summarizes values of D (left) and range (right) for all trajectories derived from HA-β_1AR–expressing (blue) or HA-β_2AR–expressing (red) H9c2 cells as cumulative distribution functions (the probability distribution of the variables D and range for complete data sets). The continuous nature of cumulative distributions for both receptor populations indicates that similar diffusive behavior presumably describes the motion of HA-β_1AR and of HA-β_2AR. The median values of D and range for both receptors were ~0.001 $\mu m^2/s$ and ~0.03 μm, respectively, similar to values obtained for other proteins that demonstrate confined diffusion, including the cystic fibrosis transmembrane conductance regulator (CFTR; Haggie *et al.*, 2006) and orthogonal array–associated aquaporin-4 (Crane *et al.*, 2008). To verify that the Qdot-labeling strategy was not responsible for receptor confinement, experiments were performed in which receptors were labeled with monomeric anti-HA Fab fragments and DyLight 649–conjugated secondary Fab fragments. On the basis of continuous image acquisition (10 fps, 100 ms exposure), HA-β_1AR (Figure 1E) and HA-β_2AR (Supplemental Figure S3) were qualitatively confined. Finally, experiments performed at a higher frame rate (60 fps) established that 30 fps

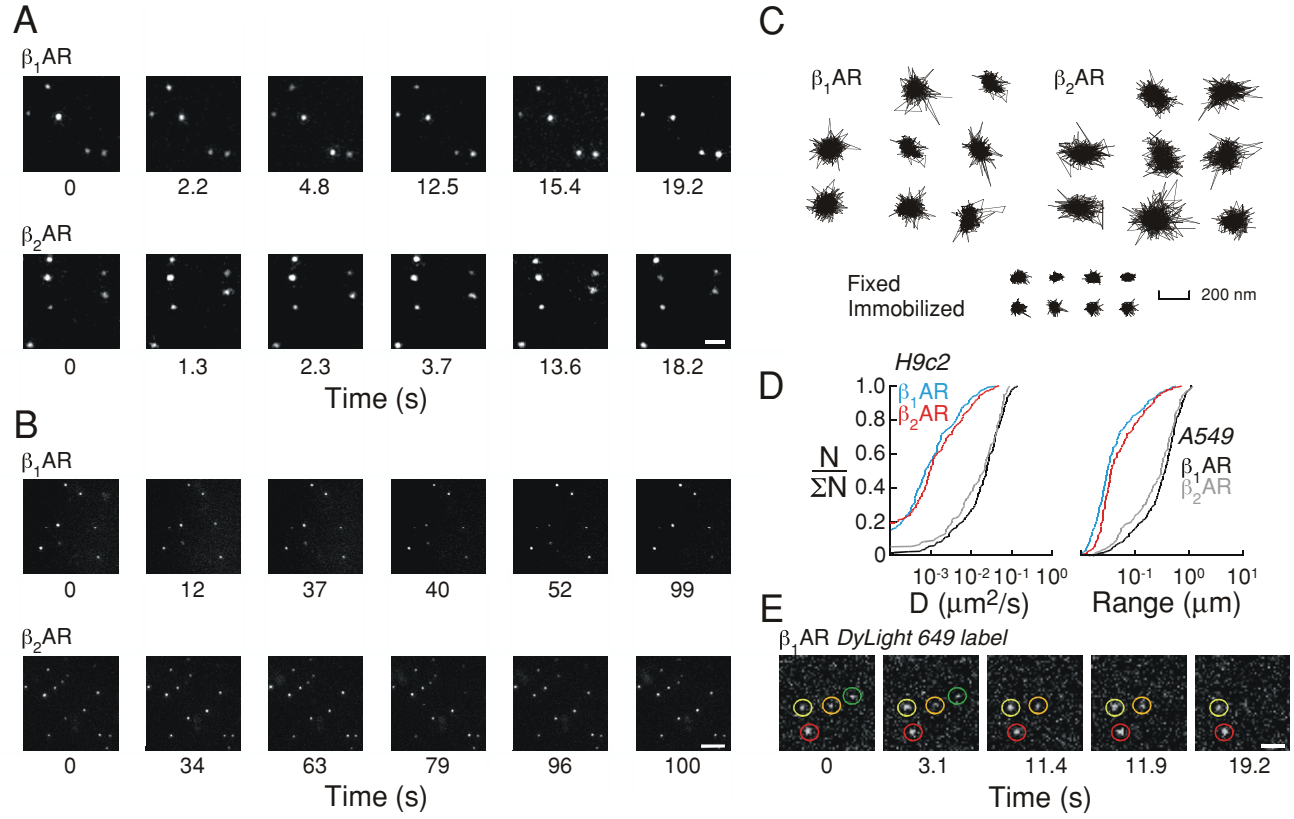

FIGURE 1: Single-particle tracking of fluorescently labeled adrenergic receptors in H9c2 cardiomyocyte-like cells. (A) Individual frames from SPT image sequences acquired continuously at 30 fps for Qdot-labeled HA-β_1AR (top) and HA-β_2AR (bottom). Scale bar, 2 μm. (B) Individual frames from time-lapse image sequences acquired at 1 fps for Qdot-labeled HA-β_1AR (top) and HA-β_2AR (bottom). Scale bar, 5 μm. (C) Representative trajectories of HA-β_1AR (left) and HA-β_2AR (right) diffusion in the plasma membrane derived from SPT experiments. Trajectories from paraformaldehyde fixed cells and immobilized Qdots are also shown (bottom). Scale bar (200 nm) applies to all trajectories. (D) Cumulative distributions of diffusion coefficient (D, left) and range at 2 s (right) for HA-β_1AR (blue) and HA-β_2AR (red) expressed in H9c2 cells and HA-β_1AR (black) and HA-β_2AR (gray) expressed in A549 alveolar epithelial cells. (E) Individual frames from image sequences of HA-β_1AR labeled with anti-HA Fab fragment and DyLight 649–conjugated secondary Fab fragment acquired continuously at 10 fps with 100 ms exposures. Labeled receptors are highlighted with colored circles; photobleaching during image acquisition reduced fluorescence associated with the green- and orange-highlighted receptors. Scale bar, 2 μm.

data sampling adequately describes receptor diffusion (unpublished data).

HA-β_1AR and HA-β_2AR were expressed in alternative cell types to determine whether confinement of these receptors in H9c2 cells was a common finding. When expressed in A549 alveolar epithelial cells at levels similar to those studied in H9c2 cells, β_1AR (Figure 1D, black; see Supplemental Movie S3) and β_2AR (Figure 1D, gray; see Supplemental Movie S4) showed relatively unhindered diffusion. Similar receptor mobility was observed in COS7 kidney fibroblasts (unpublished data). The median values of D and range for βAR diffusion in A549 and COS7 cells were ~0.02 μm^2/s and ~0.3 μm, respectively ($p < 0.005$ for D and range for both HA-βARs in H9c2 cells vs. when expressed in A549 or COS7 cells), similar to prior measurements of β_2AR diffusion in A549 cells (Hegener *et al.*, 2004) and to freely diffusing transmembrane proteins such as aquaporin-1 (Crane and Verkman, 2008).

PDZ domain interactions contribute to the confinement of β_1AR and β_2AR

The confined diffusion of HA-β_1AR and HA-β_2AR is consistent with the concept that receptors stably associate with relatively static protein complexes in the plasma membrane. As such, a series of experimental maneuvers were performed to investigate the roles of putative scaffold proteins in receptor tethering. The carboxy-termini of β_1AR (residues Glu-Ser-Lys-Val) and β_2AR (residues Asp-Ser-Leu-Leu) constitute class I PDZ-binding motifs (with the consensus X-[Ser/Thr]-X-[Val/Ile/Leu], where X is any amino acid) that selectively interact with PDZ-domain proteins. Scaffold proteins with PDZ domains are modular and typically contain domains that mediate protein complexation and/or cytoskeletal interaction (Hall and Lefkowitz, 2002; Feng and Zhang, 2009). If PDZ interactions are involved in βAR confinement, we reasoned that overexpressed PDZ domains (lacking protein/cytoskeleton–interacting domains) that selectively bind to β_1- or β_2AR would compete with endogenous PDZ-domain proteins to release receptors from complexes and reduce receptor confinement (see Figure 2A for schematic representation of this strategy). A similar experimental strategy was previously used to investigate the role of EBP50 in the confinement of CFTR (Haggie *et al.*, 2006).

To probe β_1AR PDZ interactions, the third PDZ domain of SAP97, which interacts with the carboxy-terminus of β_1AR but not β_2AR (He *et al.*, 2006), was expressed as a green fluorescent protein (GFP)

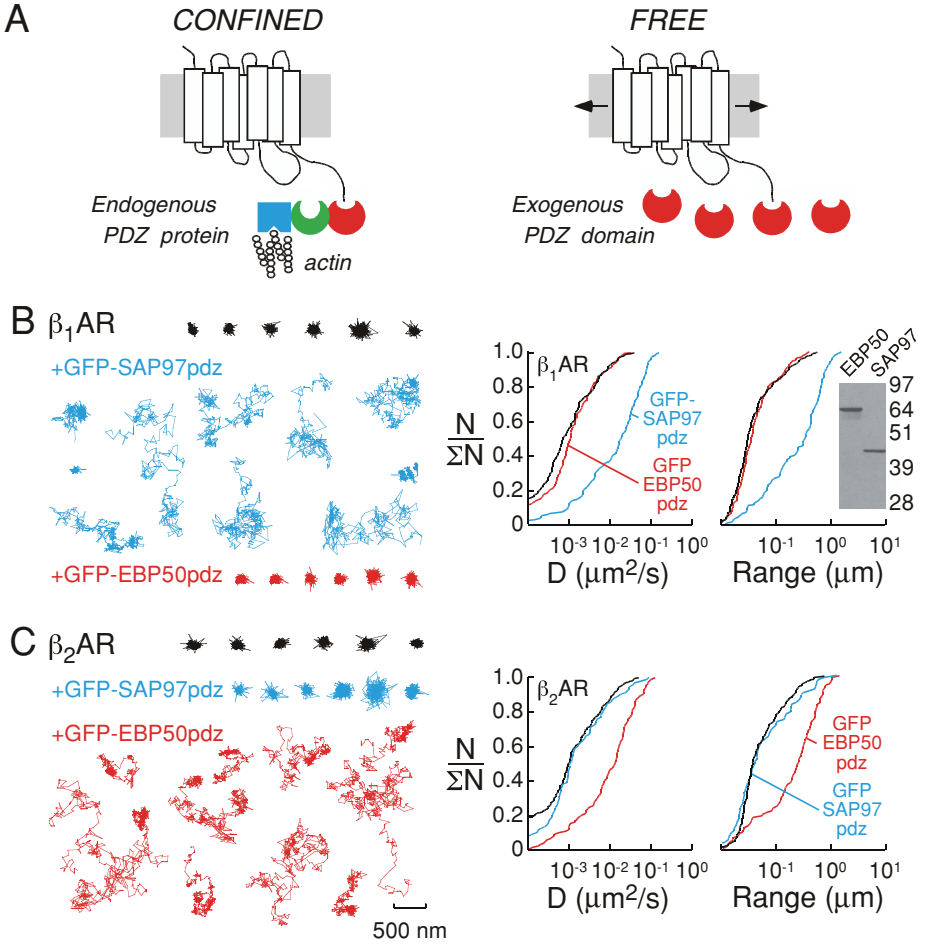

FIGURE 2: Role of PDZ-interactions in βAR confinement in H9c2 cells. (A) Schematic representation of the experimental strategy used to investigate the role of PDZ interactions in βAR confinement. Left, the carboxy-terminus of βAR interacts with a (hypothetical) endogenous scaffold protein that contains an interacting PDZ domain (red), an additional protein–protein interaction domain (green), and an actin-interacting domain (blue), which governs receptor confinement. Right, isolated PDZ domains (red) compete for the βAR carboxy-terminus and reduce receptor confinement (increased diffusion) if PDZ-type interactions are involved in receptor confinement. (B, C) Single-particle trajectories (left) and cumulative distributions (right) for D and range for (B) HA-β_1AR under control conditions (black) and in the presence of an interacting PDZ domain (SAP97pdz, blue) and a noninteracting PDZ domain (EBP50pdz, red) and (C) HA-β_2AR under control conditions (black) and in the presence of a noninteracting PDZ domain (SAP97pdz, blue) and an interacting PDZ domain (EBP50pdz, red). Scale bar (500 nm) applies to all trajectories. Integrity of GFP-EBP50pdz and GFP-SAP97pdz was confirmed by anti-GFP immunoblot of transfected H9c2 cell lysates (B, inset).

chimera (GFP-SAP97pdz) together with HA-tagged receptors. GFP-SAP97pdz distributed through the cytoplasm, as would be predicted for a soluble protein. Coexpression of GFP-SAP97pdz with HA-β_1AR reduced receptor confinement such that many trajectories covered micron distances (Figure 2B, left, blue trajectories; see Supplemental Movie S5) and cumulative distributions represented higher values of D and range (Figure 2B, right, blue curves, median values of D and range were 0.018 μm^2/s and 0.34 μm, respectively, $p < 0.005$, relative to control data). In a similar manner, the PDZ domains of EBP50 fused to GFP (GFP-EBP50pdz; Haggie *et al.*, 2006), which interacts with β_2AR but not β_1AR (Hall *et al.*, 1998a; He *et al.*, 2006), was expressed to investigate β_2AR-specific PDZ interactions. Expression of GFP-EBP50pdz, which also distributed throughout the cytoplasm, together with HA-β_2AR decreased receptor confinement (Figure 2C, red trajectories and curves; median values of D and range were 0.013 μm^2/s and 0.25 μm, respectively, $p < 0.005$; see Supplemental Movie S6). In contrast, coexpression of GFP-EBP50pdz with HA-β_1AR (Figure 2B, red trajectories and curves) or GFP-SAP97pdz with HA-β_2AR (Figure 2C, blue trajectories and curves) produced no apparent change in the diffusive properties of either receptor, indicating that PDZ-domain interactions are specific.

To confirm this observation, the carboxy-terminal amino acids of HA-β_1AR and HA-β_2AR were mutated to alanines to obviate association between βARs and interacting scaffold proteins that contain PDZ domains (Hall *et al.*, 1998a; He et al., 2006). The diffusion of both HA-β_1AR-V477L and HA-β_2AR-L413A was increased relative to that of the wild-type receptors (Supplemental Figure S4; $p < 0.005$ for both receptor populations). Taken together, these experiments indicate that selective PDZ–βAR interactions contribute to the tethering of βAR receptors in live H9c2 cells.

AKAP interactions contribute to the confinement β_1AR and β_2AR

Cardiac myocytes express numerous AKAPs (Ruehr *et al.*, 2004); however, a variety of experimental approaches have suggested that AKAP5 and AKAP12 interact with βARs (Nauert *et al.*, 1997; Fraser *et al.*, 2000; Fan *et al.*, 2001; Tao *et al.*, 2003; Gardner *et al.*, 2006; Shcherbakova *et al.*, 2007). Sequences within AKAP5 and AKAP12 have been identified that are responsible for receptor interaction (Fraser *et al.*, 2000; Tao *et al.*, 2003). Therefore, as for PDZ-type interactions, we reasoned that overexpressed receptor-interacting AKAP domains would disrupt receptor–AKAP association and release receptors from complexes if AKAPs participate in βAR confinement.

The amino-terminus of human AKAP5 (residues 1–107) interacts with β_2AR and, in addition, contains basic amino acid–rich regions that mediate plasma membrane association (Dell'Acqua *et al.*, 1998; Fraser *et al.*, 2000). Confocal imaging indicated that a chimera of the amino-terminus of murine AKAP5 (residues 1–105) and GFP (AKAP5at-GFP) also predominantly localized to the plasma membrane of H9c2 cells (unpublished data), as expected, given the high degree of similarity between the human and murine protein sequences. The amino-terminus of AKAP12 (residues 1–920, AKAP12at) also contains residues that mediate interaction with β_2AR and membrane localization (Tao *et al.*, 2003; Yan *et al.*, 2009) and a GFP chimera of AKAP12at (AKAP12at-GFP) localized to the plasma membrane of H9c2 cells (unpublished data). Given the membrane localization of AKAP5at-GFP and AKAP12at-GFP (as opposed to the cytoplasmic localization of PDZ-domain GFP fusion proteins), the mobility of these chimeras was investigated by photobleaching. Fluorescence recovery after bleaching was imaged by laser-scanning confocal microscopy at the plane

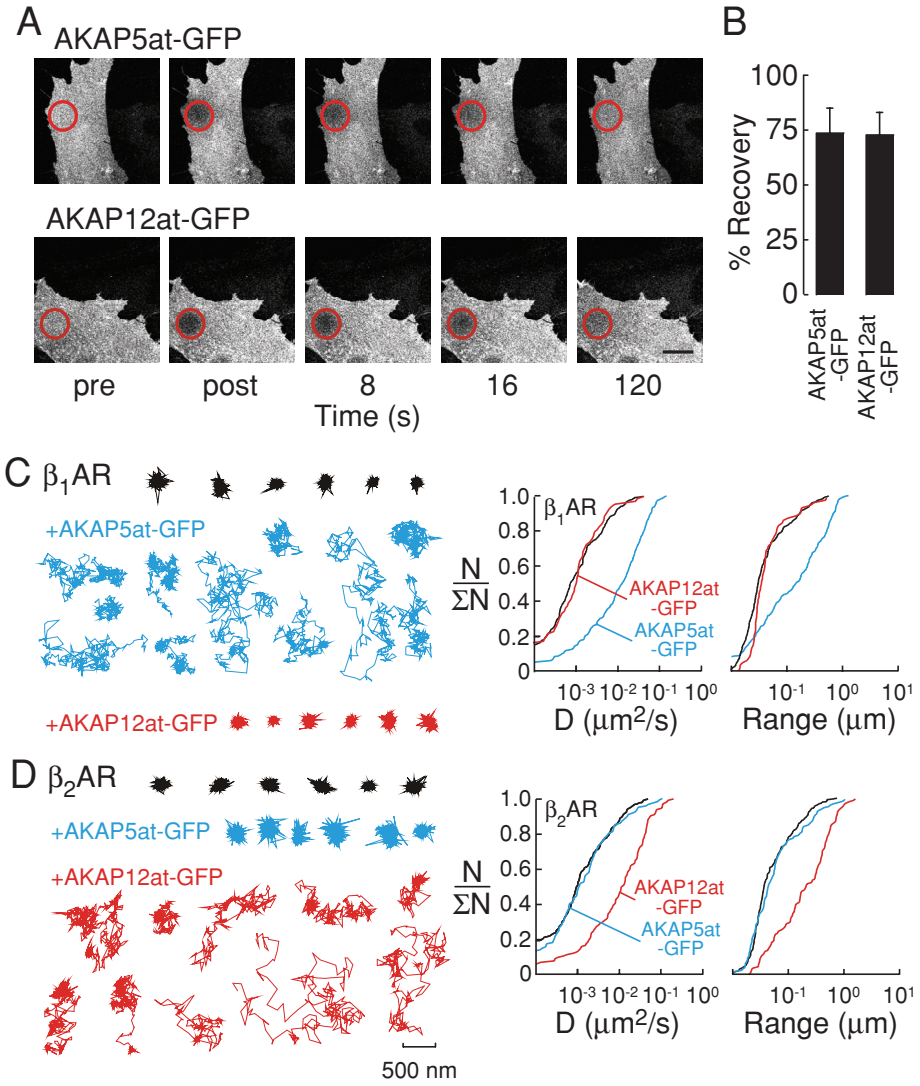

FIGURE 3: Role of AKAP interactions in βAR confinement in H9c2 cells. (A) Diffusion of AKAP amino-terminal domains measured by photobleaching with laser scanning confocal image detection of GFP chimeras. Representative image sequences are shown for AKAP5at-GFP (top) and AKAP12at-GFP (bottom); bleached regions are highlighted by red circles. Scale bar, 10 μm. (B) Fluorescence recovery of AKAP amino-terminal domain–GFP chimeras at 2 min. (C, D) Single-particle trajectories (left) and cumulative distributions (right) for D and range are shown for (C) HA-β_1AR in control conditions (black) and in the presence of AKAP5at-GFP (blue) and AKAP12at-GFP (red) and (D) HA-β_2AR under control conditions (black) and in the presence of AKAP5at-GFP (blue) and AKAP12at-GFP (red). Scale bar (500 nm) applies to all trajectories.

between cells and coverslips over a large area (~10 μm diameter) of the plasma membrane. Fluorescence recovery for AKAP5at-GFP (Figure 3A, top) and AKAP12at-GFP (Figure 3A, bottom) was observed with a recovery half-time of ~10–20 s. For both AKAP5at-GFP and AKAP12at-GFP, fluorescence recovery was ~75% complete within 2 min (Figure 3B). Therefore, as studied, the plasma membrane–associated AKAP domains cover micron distance scales within seconds, indicating that their diffusion is unhindered relative to that of βARs.

Expression of AKAP5at-GFP together with HA-β_1AR increased receptor mobility such that many trajectories covered micron distance scales (Figure 3C, left, blue trajectories) and cumulative distributions represented higher values of D and range (Figure 3C, right, blue curves; median values of D and range were 0.014 μm^2/s and 0.14 μm, respectively, $p < 0.01$). Similarly, expression of AKAP12at-GFP with HA-β_2AR decreased receptor confinement (Figure 3D, red trajectories and curves; median values of D and range were 0.013 μm^2/s and 0.21 μm, respectively, $p < 0.01$). In contrast, coexpression of AKAP12at-GFP with HA-β_1AR (Figure 3C, red trajectories and curves) or AKAP5at-GFP with HA-β_2AR (Figure 3D, blue trajectories and curves) did not change the diffusive properties of either receptor, suggesting that AKAP domain interactions were selective. A soluble β_2AR-interacting domain from AKAP12 (residues 554–938; Tao *et al.*, 2003) fused to GFP also increased β_2AR but not β_1AR diffusion (unpublished data). As such, selective AKAP–βAR interactions contribute to the tethering of βAR receptors in live H9c2 cells.

Caveolae do not participate in the confinement of β_2AR

In cardiac myocytes, caveolae have been reported to compartmentalize signal transduction pathways mediated by β_2AR but not β_1AR (Rybin *et al.*, 2000; Steinberg, 2004). Myocyte caveolae are composed of the structural protein CAV3, which forms high-order oligomeric structures (Steinberg, 2004; Parton and Simons, 2007). In contrast to PDZ-domain and AKAP proteins, specific CAV3 sequences (or specific intermediary proteins) that interact with β_2AR have not been identified. Maneuvers were designed to modulate the surface levels of CAV3, and the effects of these perturbations on β_2AR dynamics were characterized by SPT.

Although various small inhibitory RNA approaches were attempted, expression of CAV3 in H9c2 cells could not be reduced reliably. However, expression of CAV3-P104L, a dominant-negative CAV3 mutant that is retained in the Golgi and causes limb girdle muscular dystrophy (Galbiati *et al.*, 1999), dramatically reduced surface expression of CAV3 (unpublished data). In H9c2 cells, a chimera of CAV3-P104L and GFP (CAV3-P104L-GFP) was also observed in perinuclear regions that colocalized with the Golgi marker GM130 (Figure 4A, top) and retained essentially all endogenous CAV3 in the Golgi (Figure 4A, bottom; see Supplemental Figure S5B for additional images). Quantitative image analysis of CAV3-P104L-GFP–expressing cells immunostained for CAV3 indicated that ~90% of CAV3 was retained in the Golgi (Figure 4B), a value that is comparable to many knockdown approaches. Expression of CAV3-P104L-GFP did not result in Golgi retention of HA-β_2AR (Supplemental Figure S5C). In contrast, expression of CAV3-P104L-mCherry resulted in Golgi retention of dysferlin (Supplemental Figure S5D), a protein previously shown to interact with CAV3 (Hernández-Deviez *et al.*, 2006).

Single-particle tracking experiments to measure HA-β_2AR mobility in cells expressing CAV3-P104L-GFP reveal that receptor diffusion was not apparently altered by dramatic removal of surface

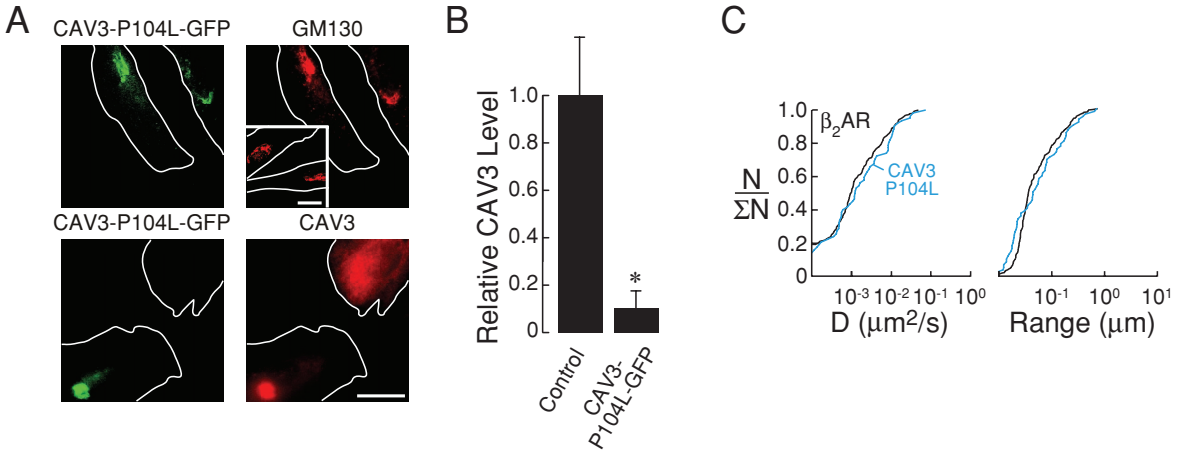

FIGURE 4: Reduced levels of caveolin-3 at the plasma membrane do not alter β_2AR confinement. (A) Fluorescence micrographs of H9c2 cells expressing CAV3-P104L-GFP (left) immunostained for GM130 (right, top) or CAV3 (which identifies endogenous CAV3 and CAV3-P104L-GFP; right, bottom). Inset (right, top), shows untransfected cells immunostained for GM130, indicating that CAV3-P104L-GFP expression did not alter Golgi morphology. Green fluorescence represents GFP fluorescence from the CAV3-P104L-GFP moieties. Cell outlines (white) were traced from transmission images. Scale bar, 10 μm. (B) Quantitative image analysis of CAV3 levels (assessed by immunocytochemistry) in non-Golgi regions of control cells and cells expressing CAV3-P104L-GFP; *$p < 0.001$. (C) Cumulative distributions of D (left) and range (right) for β_2AR under control conditions (black) and in the presence of CAV3-P104L-GFP (blue).

caveolae (Figure 4C, blue). As such, surface levels of CAV3 can be significantly reduced without altering the confinement of β_2AR.

A prerequisite for caveolar-mediated β_2AR confinement is that caveolae would also be largely immobile. A prior study in HeLa cells, which express caveolin-1 (CAV1), indicated that CAV1-GFP–labeled caveolae are relatively static and that increased CAV1-GFP expression levels could increase caveolar mobility (Pelkmans and Zerial, 2005). Therefore, the plasma membrane dynamics of caveolae and the effect of CAV3 expression levels on caveolar dynamics were characterized in H9c2 cells. To visualize caveolae in live cells, a CAV3-GFP fusion was generated, similar to an extensively studied and functional CAV1-GFP fusion (Pelkmans and Zerial, 2005).

Initially, studies were conducted in which cells were transfected to express low levels of CAV3-GFP. Transfected cells were visualized using total internal reflection fluorescence (TIRF) imaging that selectively illuminates the plasma membrane and cortical cytoplasm (imaging depth is ~150–200 nm). Caveolae labeled with CAV3-GFP could be visualized as discrete, diffraction-limited fluorescent punctae (Figure 5A), consistent with a reported size of ~100–200 nm (Parton and Simons, 2007). The appearance of CAV3-GFP–labeled caveolae was similar to that of endogenous immunostained CAV3 in H9c2 cells visualized by TIRF, suggesting that the GFP moiety did not interfere with CAV3-GFP localization (unpublished data). To verify that CAV3-GFP was associated with cholesterol-rich membrane domains by standard biochemical criteria, Triton X-100–soluble (S) and Triton X-100–insoluble (P) cellular fractions were prepared (Song *et al.*, 1997; Galbiati *et al.*, 1999). SDS–PAGE–resolved extracts from untransfected cells immunoblotted for CAV3 (Figure 5C, lanes 1 and 2) verified that CAV3 (~17 kDa) was insoluble in Triton X-100, as previously described (Galbiati *et al.*, 1999). In cells expressing low levels of CAV3-GFP, both CAV3 and CAV3-GFP (~44 kDa) were also largely isolated in Triton X-100–insoluble fractions (Figure 5C, lanes 3 and 4), indicating that CAV3 and CAV3-GFP were present in the same membrane environment. TIRF image sequences acquired at 10 fps demonstrated that the majority of labeled caveolae (~80%) were essentially static in the plasma membrane over time scales of tens of seconds (Figure 5A and Supplemental Movie S7). A small number of caveolae (~20%), however, associated with (Figure 5B, top) or dissociated from (Figure 5B, bottom) the plasma membrane (see also Supplemental Movies 8 and 9). As such, the diffusive behavior of caveolae labeled with CAV3-GFP expressed at low levels in H9c2 cells was similar to that reported for CAV1-GFP–labeled caveolae in HeLa cells (Pelkmans and Zerial, 2005) and consistent with a possible role in β_2AR scaffolding.

When H9c2 cells were transfected to express high levels of CAV3-GFP, the behavior of caveolae was very different. CAV3-GFP–labeled caveolae were still visible by TIRF imaging as bright fluorescent punctae (Figure 5D); however, significant fluorescence was also observed diffusely throughout the plasma membrane. CAV3-GFP was also detected in both Triton X-100 –soluble and Triton X-100–insoluble fractions (Figure 5C, lanes 5 and 6), confirming that excess CAV3-GFP was incompletely incorporated into cholesterol-rich membrane domains. An approximately threefold increase in Triton X-100–soluble endogenous CAV3 was observed in cells with high CAV3-GFP levels, indicating that endogenous CAV3 was also mistargeted. An anti-GFP immunoblot confirmed the presence of CAV3-GFP in Triton X-100–soluble fractions and the absence of soluble GFP moieties that could result from proteolytic cleavage of CAV3-GFP (Figure 5C, bottom). With the use of TIRF imaging, rapid exchange of caveolae between intracellular sites and the plasma membrane and movement of caveolae in the plane of the membrane were observed (Figure 5D and Supplemental Movie S10). In addition, photobleaching experiments using laser-scanning confocal microscopy were performed in cells expressing high levels of CAV3-GFP (Figure 5E). Bleaching was applied over a large area (~15 μm diameter) of the plasma membrane, and relatively rapid ($t_{1/2}$ ~20 s) and complete (~90% at 1 min) recovery of CAV3-GFP fluorescence was observed in all cells studied. Given that multiple processes (including lateral diffusion of caveolar and noncaveolar CAV3-GFP and trafficking events) contribute to the recovery of fluorescence, no formal characterization of CAV3-GFP diffusion was

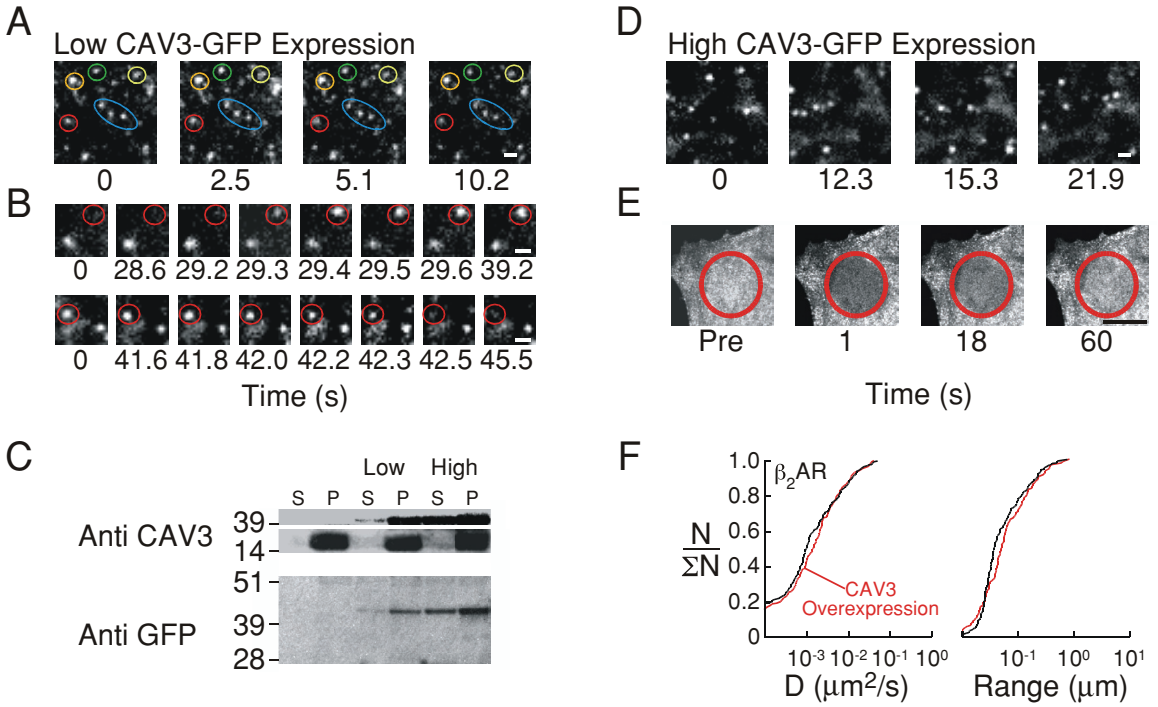

FIGURE 5: Caveolar dynamics and the role of caveolae in β_2AR confinement in H9c2 cells. Individual frames from TIRF image sequences are shown for cells expressing low levels of CAV3-GFP to illustrate (A) caveolar dynamics and (B) caveolae association (top) and dissociation (bottom) events. In A, stable caveolae are highlighted with circles, and in B, the positions of membrane association (top) and dissociation (bottom) events are highlighted. (C) Biochemical analysis of caveolin-3 solubility. Triton X-100–soluble (S) and Triton X-100–insoluble (P) cellular fractions were prepared, resolved by SDS–PAGE, and immunoblotted with anti-CAV3 antibodies (top) and anti-GFP antibodies (bottom). With anti-CAV3 antibodies, both CAV3 (~17 kDa) and CAV3-GFP (~44 kDa) were identified, whereas with anti-GFP antibodies only CAV3-GFP was identified. (D) Individual frames from TIRF image sequences are shown for a cell expressing high levels of CAV3-GFP. Contrast enhancement was applied to highlight membrane-associated caveolae, although membrane fluorescence was increased relative to cells expressing low levels of CAV3-GFP. (E) Individual frames from photobleaching experiments for cells expressing high levels of CAV3-GFP. Images were collected using confocal image detection from plasma membrane proximal to the coverslip. The bleached region is highlighted by a red circle. (F) Cumulative distributions of D (left) and range (right) for β_2AR under control conditions (black) and in the presence of high levels of CAV3-GFP (red). Scale bars, 1 μm in A, B, and D and 15 μm in E.

attempted. However, the general conclusion of these experiments is that caveolar and noncaveolar CAV3-GFP are mobile over time scales of seconds and distance scales of microns when expressed at high levels and unhindered relative to the diffusion of β_2AR.

Given the dependence of caveolar dynamics and membrane targeting on CAV3-GFP expression level, we reasoned that high levels of CAV3-GFP could also be used to assess the role of caveolae in β_2AR confinement by reducing the number of stable caveolae in the plasma membrane (and/or by competing for as-yet-unidentified proteins involved in caveolae–β_2AR interactions). The mobility of HA-β_2AR was not, however, altered by high-level expression of CAV3-GFP (Figure 5F, red). Taken together, these studies suggest that stable plasma membrane caveolae are not required for β_2AR confinement.

The actin cytoskeleton contributes to β_1AR and β_2AR confinement, and the binding capacity of β_1AR and β_2AR scaffold proteins can be saturated

The studies so far indicate that selective PDZ and AKAP interactions are involved in the confinement of βARs, and further experiments were performed to characterize these interactions. Several PDZ-domain proteins and AKAPs that associate with βARs also interact with the actin cytoskeleton, including SAP97, EBP50 (via ezrin), AKAP5, and AKAP12 (Wu *et al.*, 1998; Bretscher *et al.*, 2000; Gomez *et al.*, 2002; Malbon *et al.*, 2004). To assess the role of cytoskeletal interactions in receptor confinement, cells were treated with the actin-disrupting agent latrunculin using conditions that did not grossly alter cell morphology. The confinement of HA-β_1AR (Figure 6A, red curves and trajectories; median values of D and range were 0.012 μm^2/s and 0.20 μm, respectively, $p < 0.01$) and HA-β_2AR (Figure 6B, red curves and trajectories; median value of D and range were 0.006 μm^2/s and 0.12 μm, respectively, $p < 0.05$) was reduced by latrunculin treatment. Frick *et al.* (2007) demonstrated that latrunculin-mediated actin fragmentation does not alter the diffusive properties of proteins that do not interact with actin (thus confirming that this experimental maneuver specifically identifies proteins that interact with actin). We confirmed this finding in H9c2 cells by demonstrating that the diffusive properties of CD4-GFP, a chimeric transmembrane protein that contains no sites of actin interaction, were not altered by latrunculin treatment (Supplemental Figure S6). As such, our data indicates that the actin cytoskeleton participates in the tethering of βARs.

A prior study that investigated the plasma membrane dynamics of CFTR indicated that scaffold protein–binding capacity was saturable, such that overexpressed CFTR was not coupled to EBP50, ezrin, and the actin cytoskeleton (Haggie *et al.*, 2006). To test

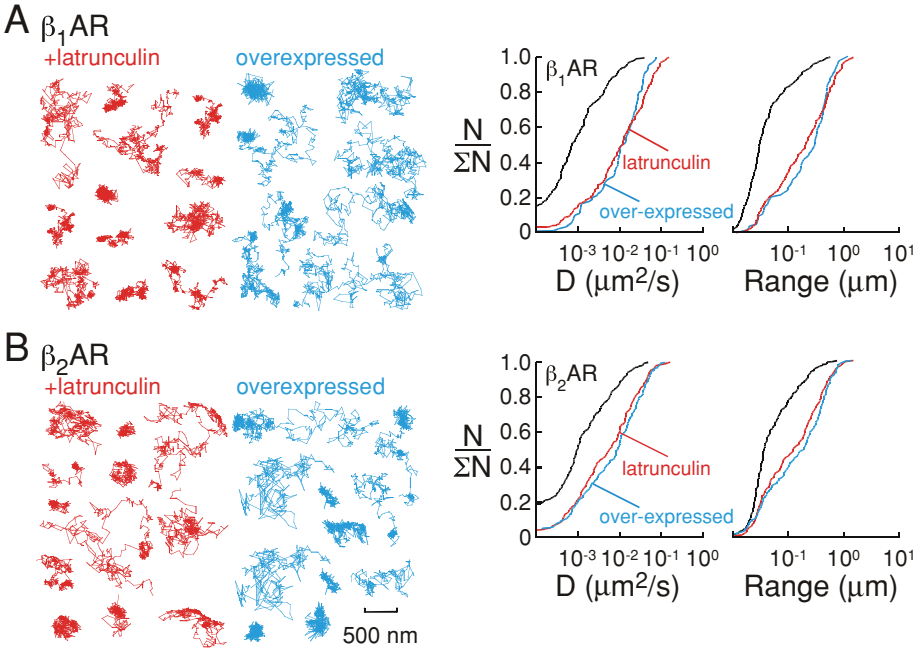

FIGURE 6: Role of the actin cytoskeleton and receptor concentration in βAR confinement. Single-particle trajectories (left) and cumulative distributions (right) for D and range are shown for (A) HA-β_1AR and (B) HA-β_2AR in the presence of latrunculin (red trajectories and curves) and under conditions in which receptor is overexpressed relative to control conditions (blue trajectories and curves). Scale bar (500 nm) applies to all trajectories.

whether the binding capacity of βAR-specific scaffold interactions could also be saturated, receptors levels were increased by altering transfection conditions (see *Materials and Methods*). In the presence of high levels of HA-tagged receptor (>25-fold overexpression of receptor), the diffusive mobility of both HA-β_1AR (Figure 6A, blue curves and trajectories; median values of D and range were 0.012 μm^2/s and 0.3 μm., respectively, $p < 0.01$) and HA-β_2AR (Figure 6B, blue curves and trajectories; median value of D and range were 0.009 μm^2/s and 0.18 μm, respectively, $p < 0.05$) was increased, indicating that a finite number of receptors can be appropriately coupled to scaffold proteins in H9c2 cells. To determine the relative capacity of receptor scaffold in H9c2 cells, increasing levels of epitope-tagged receptors were expressed and receptor mobility was determined (Supplemental Figure S7). For both HA-β_1AR and HA-β_2AR, cells were able to effectively tether receptors up to at least about threefold endogenous level.

The carboxy-terminal domains of β_1AR and β_2AR are responsible for confinement

Finally, the domains within βARs that interact with scaffold proteins in live cells were identified. Prior biochemical analysis has indicated that the carboxy-terminal domain and the third intracellular loop of βARs associate with PDZ-domain proteins and AKAPs, as well as with other proteins, including potassium channels and endophilin (Tang *et al.*, 1999; Fraser *et al.*, 2000; Fan *et al.*, 2001; Lui *et al.*, 2004). Therefore, intracellular receptor domains were expressed as soluble GFP fusions to compete with receptors for association with cytoplasmic scaffold proteins (see Figure 7A for description of the receptor regions that were expressed as GFP chimeras). Isolated cytoplasmic regions of GPCRs have been used in a variety of experimental strategies, including biochemical approaches to identify βAR-binding partners (Fraser *et al.*, 2000; Fan *et al.*, 2001), in functional assays to inhibit desensitization (Krupnick *et al.*, 1994; Mukherjee *et al.*, 1999), and in whole-cell systems to disrupt signal transduction (Borroto-Escuela *et al.*, 2010). As such, the strategy applied here to investigate βAR interactions is analogous to prior approaches, albeit with receptor diffusion used as a readout of interactions.

We initially focused on the carboxy-terminal domains of βARs, which contain PDZ-binding domains and AKAP interaction sites (Hall *et al.*, 1998a, 1998b; Fraser *et al.*, 2000; Fan *et al.*, 2001; He *et al.*, 2006). As expected, coexpression of HA-β_1AR with the soluble β_1AR carboxy-terminus domain fused to GFP (GFP-β_1ARct) resulted in reduced confinement of HA-β_1AR (Figure 7B, blue trajectories and curves; median values of D and range were 0.018 μm^2/s and 0.30 μm, respectively, $p < 0.01$), presumably in part due to competition for PDZ-binding partners. Expression of a soluble GFP chimera containing the C-terminus of β_1AR with no PDZ-binding domain (GFP-β_1ARctΔPDZ) also increased the diffusion of HA-β_1AR (Figure 7B, red; median values of D and range were 0.009 μm^2/s and 0.15 μm, respectively, $p < 0.01$), confirming that AKAP–β_1AR interactions mediate receptor confinement. In a similar manner, coexpression of HA-β_2AR with the β_2AR carboxy-terminus (GFP-β_2ARct; Figure 7C, blue; median values of D and range were 0.019 μm^2/s and 0.16 μm, respectively, $p < 0.01$) and the β_2AR carboxy-terminus with no PDZ-binding domain (GFP-β_2ARctΔPDZ; Figure 7C, red; median values of D and range were 0.007 μm^2/s and 0.16 μm, respectively, $p < 0.01$) resulted in reduced confinement of HA-β_2AR, confirming that both PDZ and AKAP interactions participate in β_2AR tethering. The cytoplasmic loop 3 region of β_2AR has been shown to interact with AKAP5 in biochemical assays (Fraser *et al.*, 2000). However, the confined diffusion of HA-β_2AR was not altered by coexpression of the β_2AR cytoplasmic loop 3 regions, suggesting that this interaction is not relevant for receptor tethering in live cells (GFP-β_2ARcl3; Figure 7C, green). Similarly, coexpression of the β_1AR cytoplasmic loop 3 regions (GFP-β_1ARcl3) did not effect the confinement of HA-β_1AR (Figure 7B, green). The cytoplasmic loop 1 and 2 regions of β_1- and β_2AR show high degrees of sequence similarity (Figure 7A), and neither region would thus be predicted to constitute a potential site of receptor-specific scaffold interactions. Therefore, the roles of these loops in receptor confinement were assessed only for β_1AR; however, neither region altered receptor diffusion (unpublished data). Coexpression of GFP-β_2ARct with HA-β_1AR (Figure 7D, left, red) or GFP-β_1ARct with HA-β_2AR (Figure 7D, right, red) did not alter the diffusion of receptors, confirming the specificity of interactions in receptor confinement. Taken together, these studies indicate that specific interactions with the cytoplasmic-exposed, carboxy-terminal regions of βARs, but not other receptor regions, mediate receptor tethering in H9c2 cells.

DISCUSSION

The primary conclusion of this study is that unstimulated β_1- and β_2ARs are confined in the plasma membrane of live H9c2 cardiomyocyte-like cells expressing relevant concentration of proposed receptor complex constituents. Interactions with PDZ-domain–containing

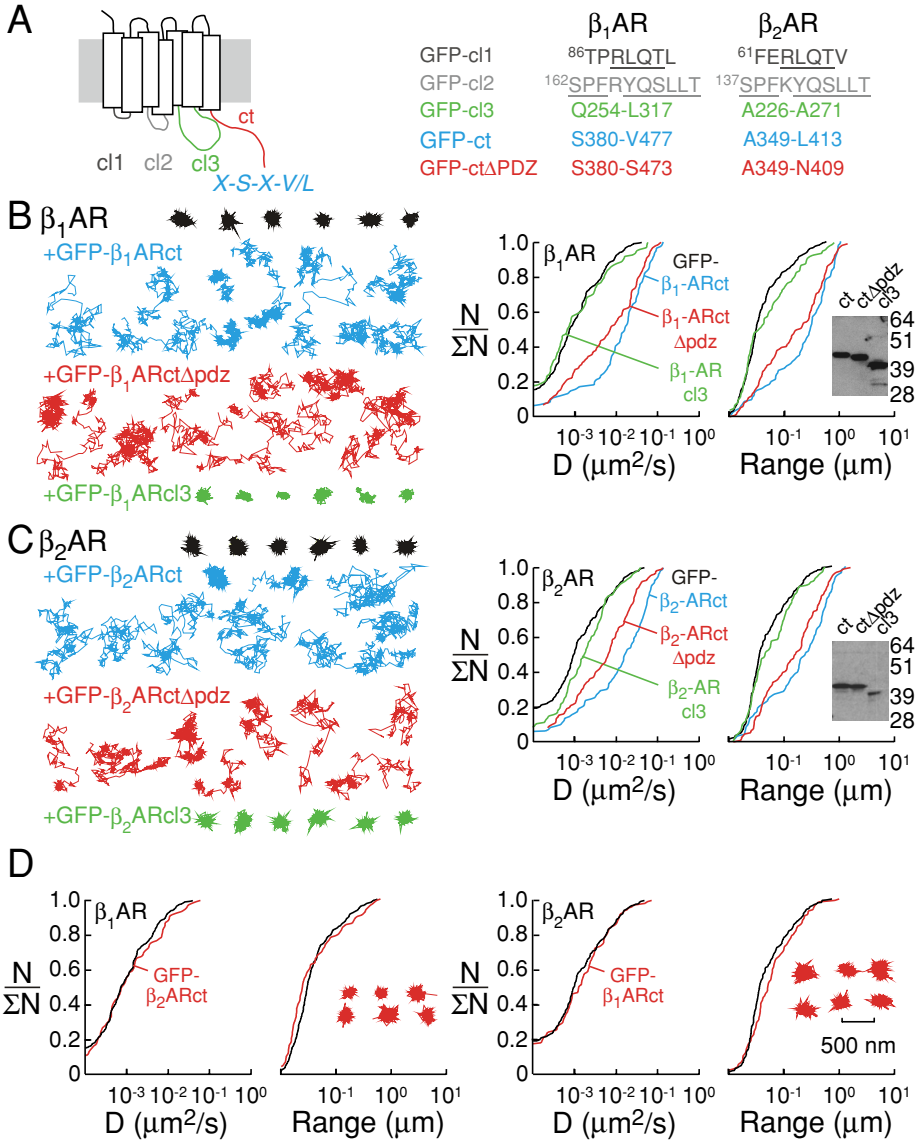

FIGURE 7: Identification of βAR domains involved in receptor confinement. (A) Schematic representation of receptor domains (left) and the specific protein sequences (right) that were expressed as soluble GFP chimeras to investigate cytoplasmic receptor domains required for scaffold interactions. Representative single-particle trajectories (left) and cumulative distribution functions (right) for D and range are shown for (B) HA-β_1AR under control conditions (black), coexpressed with a GFP chimera of the β_1AR carboxy-terminus (GFP-β_1ARct, blue), coexpressed with a GFP chimera of the β_1AR carboxy-terminus without a PDZ-binding motif (GFP-β_1ARctΔpdz, red), and coexpressed with a GFP chimera of the β_1AR cytoplasmic loop 3 region (GFP-β_1ARcl3, green) and (C) HA-β_2AR under control conditions (black), coexpressed with a GFP chimera of the β_2AR carboxy-terminus (GFP-β_2ARct, blue), coexpressed with a GFP chimera of the β_2AR carboxy-terminus without the PDZ-binding motif (GFP-β_2ARctΔpdz, red), and coexpressed with a GFP chimera of the β_2AR cytoplasmic loop 3 region (GFP-β_2ARcl3, green). (D) Cumulative distribution functions and trajectories (insets) for HA-β_1AR coexpressed with a GFP chimera of the β_2AR carboxy-terminus (GFP-β_2ARct; left, red) and HA-β_2AR coexpressed with a GFP chimera of the β_1AR carboxy-terminus (GFP-β_1ARct; right, red). Scale bar (500 nm) applies to all trajectories. Integrity of soluble GFP-β_1/β_2AR domain chimeras was confirmed by anti-GFP immunoblot of transfected H9c2 cell lysates (B and C, insets).

proteins, AKAPs, and the actin cytoskeleton were largely responsible for the immobilization of receptors. For instance, the expression of dominant-negative PDZ domains was able to disrupt receptor complexes, indicating that PDZ-type interactions tether receptors. PDZ interactions that mediated β_1- and β_2AR confinement were selective, as predicted from biochemical approaches (Hall *et al.*, 1998a, 1998b; He *et al.*, 2006). In a similar manner, overexpression of AKAP domains shown to interact with βARs was able to disrupt receptor complexes, suggesting that AKAPs participate in receptor complexation. In cardiac myocytes, AKAP interactions that confined β_1 and β_2ARs were selective, such that β_1AR interacted with AKAP5, and β_2AR associated with AKAP12. This finding contrasts with prior functional and biochemical studies that demonstrated AKAP5 association with β_2AR, albeit in different cell types (Fraser *et al.*, 2000). Treatment of cells with the actin-disrupting agent latrunculin also reduced βAR confinement, consistent with association of receptors with the actin cytoskeleton presumably via PDZ or AKAP interactions. The carboxy-terminal domain of receptors was shown to be largely responsible for receptor tethering, whereas other receptor domains were of much less or no importance in confining receptors. Prior biochemical studies indicated that the intracellular loop 3 region of β_2AR interacts with AKAP5; however, in H9c2 cells no evidence was found to support such an interaction. Our study indicates that β_1- and β_2AR are compartmentalized in live H9c2 cells at the level of their interactions with PDZ-domain proteins, AKAPs, and the actin cytoskeleton.

Previous studies implicated caveolae in the compartmentalization of β_2AR. In live H9c2 cells, caveolae were found to be largely immobile, consistent with a possible role in β_2AR tethering. Reduction of surface caveolae (by ~90%) by overexpression of a dominant-negative CAV3 mutant had no effect on β_2AR dynamics. Furthermore, the mobility and cellular distribution of caveolin-3 were dramatically altered when a CAV3-GFP fusion was overexpressed; however, this perturbation did not alter β_2AR confinement. Taken together, these findings suggest that in unstimulated H9c2 cells confinement of β_2AR does not depend on caveolae. A number of caveats exist with the interpretation of prior studies that reported β_2AR–caveolin association. Biochemical approaches generally provide no information regarding the degree or dynamics of protein association. Similarly, techniques such as isopycnic centrifugation offer limited resolution and in many instances actually demonstrate that both β_1- and β_2AR exist in overlapping membrane fractions with CAV3 (Rybin *et al.*, 2000; Balijepalli *et al.*, 2006). Functional assays in which caveolae are proposed to be disrupted selectively use compounds (e.g. filipin, cyclodextrin) that alter many cellular properties and processes and interrogate multiple steps in adrenergic signaling pathways (Hancock, 2006; Pontier *et al.*, 2008). The diffusive properties of raft-associated and non–raft-associated membrane proteins are reduced by cyclodextrin treatment, further

indicating that this treatment nonselectively alters plasma membrane properties (Kenworthy *et al.*, 2004). Finally, in a study using superresolution imaging of βARs in H9c2 cells, the vast majority of β_2ARs (~85%) were not associated with caveolae, although these data were interpreted to support the hypothesis that β_2AR–caveolae association promotes specificity in adrenergic signaling (Ianoul *et al.*, 2005). The present study does not rule out the participation of caveolae in adrenergic signaling responses upon receptor stimulation.

Increased efficiency and specificity are proposed outcomes of compartmentalized signal transduction processes; however, only a limited number of studies have directly studied spatial organization within signaling pathways. Several studies have indicated that receptors and scaffolds demonstrate relatively unhindered diffusion, inconsistent with their participation in stable multiprotein complexes. Endogenous and transfected β_2AR has been shown to be largely mobile in several cell types (Barak *et al.*, 1997; Hegener *et al.*, 2004; Yudowski *et al.*, 2006), in addition to the COS7 and A549 cells used in this study. Other GPCRs (Sergé *et al.*, 2002; Suzuki *et al.*, 2005; Hern *et al.*, 2010) and the epidermal growth factor (EGF) receptor (Lidke *et al.*, 2005; Chung *et al.*, 2010) also demonstrate relatively unhindered diffusion or short periods of immobilization (seconds) in the plasma membrane. Several neuronal receptors and PDZ scaffolds have been shown to be mobile over seconds to minutes (Choquet and Triller, 2003; Gray *et al.*, 2006; Zheng *et al.*, 2010). Protein kinase A (PKA) catalytic subunits in neurons are mobile over seconds despite AKAP-mediated confinement to dendritic shafts, suggesting low affinity of PKA–AKAP association in live cells (Zhong *et al.*, 2009). Conversely, a number of studies support the concept of compartmentalized signal transduction, particularly in activated pathways. Imaging of cAMP and Ca^{2+} transients with fluorescence resonance energy transfer (FRET)–based probes has demonstrated that second messenger concentrations can increase in localized regions of cardiac myocytes and other cell types (Zaccolo *et al.*, 2002). Live-cell imaging studies of immune cells have provided evidence that signaling molecules become clustered and immobilized upon cellular activation (Huppa and Davis, 2003; Douglass and Vale, 2005). Similarly, fluorescence imaging studies have demonstrated that activation of signaling pathways initiated by Ras, a lipidated G protein, and CD59, a glycosylphosphatidylinositol–anchored receptor, proceeds via transient immobilization (seconds) and nanoscale clustering of signaling molecules (Murakoshi *et al.*, 2004; Kholodenko *et al.*, 2010). Together, these studies provide evidence that compartmentalization of signaling is a physiologically relevant phenomenon, but that confinement of signaling components is not a default mechanism. These studies also suggest that dynamic analysis of receptors and scaffolds in live cells, in addition to biochemical and functional studies, may be necessary to formally conclude that confinement mechanisms occur within signaling pathways.

Spatial confinement of proteins can be mediated by several mechanisms. Interactions with actin-associated PDZ and/or AKAP scaffolds have been shown to confine the diffusion of CFTR (Haggie *et al.*, 2006), in addition to the βARs studied here. The actin cytoskeleton has also been shown to participate in the confinement of caveolae and nanoscale protein clusters such as those observed during Ras activation (Murakoshi *et al.*, 2004; Pelkmans and Zerial, 2005). The M23 form of the aquaporin-4 water channel forms largely immobile oligomeric complexes; however, confinement of these structures (over minutes) is not influenced by actin but does involve PDZ-type interactions (Crane *et al.*, 2008). In activated T-cells, the confinement of protein clusters containing CD2 (a non–raft-associated coreceptor) is mediated by protein–protein association with scaffold proteins and does not involve actin (Douglass and Vale, 2005). Lipid microdomains have been proposed to mediate protein confinement; however, several biophysical approaches such as FRET and photobleaching have provided evidence against this hypothesis (Glebov and Nichols, 2004; Kenworthy *et al.*, 2004; Douglass and Vale, 2005). In the case of β_1- and β_2AR, the present study suggests that receptor confinement is determined by the affinities, number, and association/dissociation rates of specific scaffold proteins. Overexpression of β_1- and β_2AR in H9c2 cardiomyocyte-like cells resulted in increased receptor diffusion, presumably due to saturation of the binding capacity of scaffold proteins. This observation suggests that receptor–scaffold interactions are unlikely to be fully recapitulated in cell systems in which receptors are highly overexpressed. When studied in A549 and COS7 cells, β_1- and β_2ARs demonstrated relatively unhindered mobility, most likely due to the absence or reduced concentration of scaffold proteins. For instance, COS7 and A549 cells express EBP50 and SAP97 but lack many AKAPs (Naren *et al.*, 2003; Oliveria *et al.*, 2003; Pieretti *et al.*, 2003; Bossard *et al.*, 2006).

In summary, our study provides direct evidence that unstimulated β_1- and β_2AR are immobilized in the plasma membrane of H9c2 cardiomyocyte-like cells. Complexation is mediated by carboxy-terminal PDZ domain and AKAP interactions and not by association with caveolae. Immobilization of βARs presumably contributes to the spatial segregation of signal transduction components and consequent specificity of cardiac adrenergic pathways.

MATERIALS AND METHODS

Plasmid constructs

cDNA constructs containing β_1AR and β_2AR with amino-terminal HA-epitope tags have been used extensively and previously described (Cao *et al.*, 1999; Xiang *et al.*, 2002a). Receptor mutants in which the C-terminal residue was mutated to an alanine residue were generated using standard PCR-based techniques, and the complete sequence of mutants was confirmed. The GFP-EBP-50pdz construct has been previously described (Haggie *et al.*, 2006) and consists of GFP ligated to the two PDZ domains of EBP50 (residues 1–325) but lacks the C-terminal ezrin-binding domain of EBP50 (residues 326–355). To generate GFP-SP97pdz, the third PDZ domain of SAP97 (residues 459–607, provided as a 6-his-tagged domain by Randy Hall, Emory University School of Medicine, Atlanta, GA; He *et al.*, 2006) was PCR amplified and inserted in pEGFP-C1 (Clontech, Mountain View, CA). To generate AKAP5at-GFP, the N-terminus of AKAP5 (residues 1–105) was PCR amplified (using a plasmid containing full-length AKAP5-GFP as template, a generous gift from Brigitte Blackman, University of California, San Francisco, San Francisco, CA) and inserted in pEGFP-N1 (Clontech). The AKAP12at-GFP plasmid (AKAP12 residues 1–920 fused to the N-terminus of GFP) was a generous gift from Bryon Grove (University of North Dakota, Grand Forks, ND) and has been described (Yan *et al.*, 2009). cDNA for murine CAV3 was purchased from the American Type Culture Collection (ATCC, Manassas, VA), PCR amplified, and ligated into pEGFP-N1 (Clontech) to generate CAV3-GFP. The CAV3-P104L and CAV3-P104L-GFP mutants of CAV3 were generated using the QuikChange II Site-Directed Mutagenesis Kit (Stratagene, Santa Clara, CA). To generate soluble GFP chimeras of cytoplasmic-facing regions of β_1AR and β_2AR, appropriate receptor sequences were identified (based on crystallographic data and literature precedents), PCR amplified, and ligated into pEGFP-C1 (Clontech). The location of these regions, which represent the three intracellular loop regions,

the full carboxy-terminus, and the carboxy-terminus lacking the PDZ-binding domain (four residues), within the βARs and the precise protein sequences that were considered are presented in Figure 7A. CD4-GFP was a generous gift from Gergely Lukacs (McGill University, Montreal, Canada) and contains the extracellular and transmembrane domains of CD4 ligated to GFP. A construct encoding GFP fused to the amino-terminus of dysferlin was a generous gift from Kate Bushby (Newcastle University, Newcastle upon Tyne, United Kingdom; Hernández-Deviez *et al.*, 2006).

Cell culture, transfection, and treatments

Rat H9c2(2-1) cells, which show myoblast morphology and were originally isolated from embryonic heart myocardium, were purchased from the ATCC (ATCC number CRL-1446). This cell type shares several phenotypic properties with cardiac myocytes and was used in several prior studies that investigated adrenergic signaling complexes or processes in heart cells (for example, see Ianoul *et al.*, 2005). Cells were cultured on 18-mm coverglasses in 12-well plates for experiments and were transfected using Lipofectamine 2000 (Invitrogen, Carlsbad, CA) with 1 μg of plasmid. Expression levels of HA-βARs and CAV3-GFP were controlled by using defined amounts of receptor (0.01–0.02 μg) or CAV3-GFP (0.05 μg) encoding plasmids together with pcDNA3.1 or plasmids encoding GFP chimeras (as described in *Results*) in a total of 1 μg of DNA. To overexpress HA-βARs or CAV3-GFP, cells were transfected with 50-fold more plasmid encoding HA-tagged receptor or 20-fold more plasmid encoding CAV3-GFP in a total of 1 μg of plasmid. To fragment the actin cytoskeleton, cells were treated with 0.5 μM latrunculin B for 10 min before and during tracking experiments. A549 human alveolar epithelial cells and COS7 monkey kidney fibroblast cells were acquired from the University of California, San Francisco, Cell Culture Facility and cultured using standard conditions.

Immunostaining and biochemistry

To establish levels of adrenergic receptor overexpression in H9c2 cells expressing either HA-β_1AR or HA-β_2ARs, a two-step immunostaining protocol was established. For cells expressing HA-β_1AR, transfected cells were identified by immunostaining with anti-HA antibody (16B12; Covance, Berkeley, CA) and Alexa Fluor 555–conjugated secondary antibody and β_1AR levels were assessed with anti-β_1AR antibody (ab3546; Abcam, Cambridge, MA) and Alexa Fluor 488–labeled secondary antibody. For HA-β_2AR–expressing cells, transfected cells were also identified with anti–HA antibody/Alexa Fluor 555–conjugated secondary antibody staining, and total β_2AR was assessed with anti-β_2AR antibody (ab13989; Abcam) and Alexa Fluor 488–labeled secondary antibody. Given that overall transfection efficiencies were relatively low in H9c2 cells, this protocol allowed comparison of adrenergic receptor levels in adjacent transfected (containing HA-$\beta_{1\text{ or }2}$AR and endogenous $\beta_{1\text{ or }2}$AR [Alexa Fluor 555 and Alexa Fluor 488 fluorescence]) and nontransfected (endogenous $\beta_{1\text{ or }2}$AR only [Alexa Fluor 488 fluorescence only]) cells. Standard image analysis methods were applied to quantify receptor levels in transfected and nontransfected cells by comparison of background-corrected Alexa Fluor 488 intensities, and data were derived from 30–40 cells. Images were acquired using a Nikon TE2000E microscope equipped with an EXFO X-Cite, Nikon 60× numerical aperture (NA)–1.45 TIRF objective lens and high-sensitivity QuantEM:512SC charge-coupled device (CCD) camera (Photometrics, Tucson, AZ). Given the low levels of HA-tagged receptors and high levels of cellular autofluorescence, the ~50% increase (1.5-fold total receptor levels in transfected cell) represented a minimal level that could be accurately quantified.

Cells transiently transfected to express CAV3-P104L-GFP were fixed, permeabilized, and immunostained with anti-CAV3 antibody (ab30750; Abcam) and Alexa Fluor 555–conjugated secondary antibody to quantitatively determine the effects of CAV3-P104L-GFP expression on non-Golgi CAV3 levels. Analysis of images acquired by wide-field fluorescence microscopy was used to calculate background-corrected, area-integrated Alexa Fluor 555 intensities in non-Golgi regions (areas 6–10 μm away from the nucleus; see Supplemental Figure S5A) of cells that expressed and did not express CAV3-P104L-GFP. Given that wide-field fluorescence imaging was used and that CAV3-associated fluorescence could be detected from all cellular compartments (including the plasma membrane, trafficking vesicles, and compartments in which CAV3 is synthesized), the ~90% reduction in CAV3 levels in non-Golgi regions of CAV3-P104L-GFP–expressing cells potentially represents an overestimate of the CAV3 levels present at the cell surface.

Triton X-100–soluble and Triton X-100–insoluble cell fractions were prepared as described (Song *et al.*, 1997), and equal amounts of soluble and insoluble proteins were resolved on Bis-Tris PAGE gels (Invitrogen). To verify the integrity of GFP chimeras used in experiments, transfected cells were lysed using RIPA buffer and resolved on Bis-Tris PAGE gels. CAV3 was immunoblotted using antibody ab30750 (Abcam). GM130 was immunostained using antibody ab52649 (Abcam). GFP was immunoblotted with polyclonal antibody ab290 (Abcam).

Live-cell imaging experiments and analysis

For all live-cell imaging, cells were mounted in custom fabricated chambers, bathed in phosphate-buffered saline supplemented with 6 mM glucose and 1.1 mM pyruvate, and maintained at 37°C with a microincubator (Harvard Apparatus, Holliston, MA) and objective lens heater (Bioptechs, Butler, PA). SPT experiments with Qdot) labeling were performed using a Nikon TE2000U microscope equipped with an EXFO X-Cite light source, Nikon 100× NA-1.45 TIRF objective lens, and Hamamatsu (Hamamatsu City, Japan) C9100 EM-CCD camera. Data were typically acquired at 30 fps, and the lateral resolution of the system, defined as the standard deviation of centroid positions derived from immobilized Qdots, was ~14 nm. HA-β_1AR–, HA-β_2AR–, HA-β_1AR-V477A–, and HA-β_2AR-L413A–expressing cells were labeled with anti-HA antibody (HA.11 Clone 16B12; Covance), biotin-conjugated goat anti–mouse Fab fragment (Jackson ImmunoResearch Laboratories, West Grove, PA), and streptavidin-conjugated Qdots emitting at 655 nm (Invitrogen). CD4-GFP–expressing cells were labeled with anti–human CD4 antibody (Invitrogen), biotin-conjugated goat anti–mouse Fab fragment (Jackson ImmunoResearch), and streptavidin-conjugated Qdots emitting at 655 nm (Invitrogen). Trajectories describing receptor motions were reconstructed from image sequences using IDL algorithms, and quantitative analysis of trajectories was performed using LabView algorithms (Haggie *et al.*, 2006; Crane and Verkman, 2008). For all SPT experiments, data presented in this study were derived from two to six independently transfected sets of cells, and cumulative distributions are compiled from 62–315 individual trajectories generated from >10 cells (for HA-β_1AR–expressing cells, the average number of trajectories per maneuver was 173, and for HA-β_2AR–expressing cells, the average number of trajectories per maneuver was 132). In all instances, cumulative distribution plots represent complete data sets. Statistical analysis was performed using the nonparametric Kolmogorov–Smirnov test. For maneuvers that produced statistically significant data relative to control conditions, D and range were always both significant (and often identical); as such, p values of lowest significance are quoted for either D or

range for all significant data sets. Time-lapse imaging was performed at 1 fps using 100 ms acquisitions and shuttered illumination, and experiments were performed on >12 cells. Imaging of receptor labeled with anti-HA Fab fragment (generated from HA.11 antibody using Fab Preparation Kit; Pierce, Thermo Fisher Scientific, Rockford, IL) and DyLight 649–conjugated secondary Fab (Jackson ImmunoResearch) was performed using a Nikon TE2000E microscope equipped with an EXFO X-Cite, Nikon 100× NA-1.49 TIRF objective lens, Cy5 filter set (Chroma Technology, Bellows Falls, VT), QuantEM:512SC CCD (Photometrics), and autofocus system. Data were acquired continuously at 10 fps (100 ms acquisitions) over 20 s from 7–10 cells. As was observed with Qdot-labeling strategies, nonspecific labeling of untransfected cells with anti-HA Fab fragments was near zero. Total internal reflection fluorescence was performed using a Nikon TE2000E microscope with a 488 nm argon-ion laser, 60× NA-1.49 TIRF objective lens, Z488/10X, Z488RDC, and ET525/50M filters (Chroma), QuantEM:512SC CCD, and autofocus system. The point spread function of this microscope system was determined using 40 nm FluoSpheres emitting at 515 nm (Invitrogen). Data for caveolae dynamics were acquired from 10–12 cells. Laser scanning confocal microscopy was performed using a Nikon FN-S2N microscope equipped with a Nikon D-Eclipse CI confocal module, 488 nm argon-ion laser, and Nikon 100× NA-1.49 TIRF objective lens. Data for AKAP diffusion were derived from 8–10 individual cells.

ACKNOWLEDGMENTS

We thank Randy Hall, Kate Bushby, Bryon Grove, Brigette Blackman, Gergely Lukacs, and Mark von Zastrow for supplying plasmid constructs. We thank A. S. Verkman, Florian Baumgart, Jonathan Crane, and Tobias Moritz for their comments and helpful discussions regarding the manuscript. This study was supported by National Institutes of Health Grant DK 081355 and a Beginning Grant-in-Aid from the American Heart Association (0765070Y).

REFERENCES

Balijepalli RC, Foell JD, Hall DD, Hell JW, Kamp TJ (2006). Localization of cardiac L-type Ca^{2+} channels to a caveolar macromolecular signaling complex is required for β_2-adrenergic regulation. Proc Natl Acad Sci USA 103, 7500–7505.

Barak LS, Ferguson SG, Zhang J, Martenson C, Meyer T, Caron MG (1997). Internal trafficking and surface mobility of a functionally intact β2-adrenergic receptor–green fluorescent protein conjugate. Mol Pharmacol 51, 177–184.

Borroto-Escuela DO, Correia PA, Perez Alea M, Narvaez M, Garriga P, Fuxe K, Ciruela F (2010). Impaired M3 muscarinic acetylcholine receptor signal transduction through blockade of binding of multiple proteins to its third intracellular loop. Cell Physiol Biochem 25, 397–408.

Bossard F, Robay A, Toumaniantz G, Dahimene S, Becq F, Merot J, Gauthier C (2006). NHE-RF1 protein rescues ΔF508-CFTR function. Am J Physiol Lung Cell Mol Physiol 292, L1085–L1094.

Bretscher A, Chambers D, Ngyuyen R, Reczek D (2000). ERM-Merlin and EBP50 protein families in plasma membrane organization and function. Annu Rev Cell Dev Biol 16, 113–143.

Cao TT, Deacon HW, Reczek D, Bretscher A, von Zastrow M (1999). A kinase-regulated PDZ-interaction controls endocytic sorting of the β_2-adrenergic receptor. Nature 401, 286–290.

Choquet D, Triller A (2003). The role of receptor diffusion in the organization of the postsynaptic membrane. Nat Rev Neurosci 4, 251–265.

Chung I, Akita R, Vandlen R, Toomre D, Schlessinger J, Mellman I (2010). Spatial control of EGF receptor activation by reversible dimerization on living cells. Nature 464, 783–787.

Crane JM, Van Hoek AN, Skach WR, Verkman AS (2008). Aquaporin-4 dynamics in orthogonal arrays in live cells visualized by quantum dot single particle tracking. Mol Bio Cell 19, 3369–3378.

Crane JM, Verkman AS (2008). Long-range nonanomalous diffusion of quantum dot-labeled aquaporin-1 water channels in the cell plasma membrane. Biophys J 94, 702–713.

Dell'Acqua ML, Faux MC, Thorburn J, Thorburn A, Scott JD (1998). Membrane-targeting sequences on AKAP79 bind phospatidylinositol-4,5-bisphosphate. EMBO J 17, 2246–2260.

Douglass A, Vale RD (2005). Single-molecule microscopy reveals plasma membrane microdomains created by protein-protein networks that exclude or trap signaling molecules in T cells. Cell 121, 937–950.

Fan G, Shumay E, Wang HH, Malbon CC (2001). The scaffold protein gravin (AKAP250) binds β_2-adrenergic receptor via the receptor cytoplasmic R329-L413 domain and provides a mobile scaffold during desensitization. J Biol Chem 276, 24005–24014.

Feng W, Zhang M (2009). Organization and dynamics of PDZ-domain-related supramodules in the postsynaptic density. Nat Rev Neurosci 10, 87–99.

Fraser IDC, Cong M, Kim JY, Rollins EN, Daaka Y, Lefkowitz RJ, Scott JD (2000). Assembly of an A kinase-anchoring protein–β2-adrenergic receptor complex facilitates receptor phosphorylation and signaling. Curr Biol 10, 409–412.

Frick M, Schmidt K, Nichols BJ (2007). Modulation of lateral diffusion in the plasma membrane by protein density. Curr Biol 17, 462–467.

Galbiati F, Volonté D, Minetti C, Chu JB, Lisanti MP (1999). Phenotypic behavior of caveolin-3 mutations that cause autosomal dominant limb girdle muscular dystrophy. J Biol Chem 274, 25632–25641.

Gardner LA, Travalin SJ, Goehring AS, Scott JD, Bahouth SW (2006). AKAP79-mediated targeting of the cyclic AMP-dependent protein kinase to the β_1-adrenergic receptor promotes recycling and functional resensitization of the receptor. J Biol Chem 281, 33537–33553.

Glebov OO, Nichols BJ (2004). Lipid raft proteins have a random distribution during localized activation of the T-cell receptor. Nat Cell Biol 6, 238–243.

Gomez LL, Alam S, Smith KE, Horne E, Dell'Acqua ML (2002). Regulation of A-kinase anchoring protein 79/150-cAMP-dependent protein kinase postsynaptic targeting by NMDA receptor activation of calcineurin and remodeling of dendritic actin. J Neurosci 22, 7027–7044.

Gray NW, Weimer RM, Bureau I, Svoboda K (2006). Rapid redistribution of synaptic PSD-95 in the neocortex in vivo. PLoS Biol 4, e370.

Haggie PM, Kim JK, Lukacs GL, Verkman AS (2006). Tracking of quantum dot-labeled CFTR shows near immobilization by C-terminal PDZ interactions. Mol Biol Cell 17, 4937–4945.

Hall RA, Lefkowitz RJ (2002). Regulation of G protein-coupled receptor signaling by scaffold proteins. Circ Res 91, 672–212.

Hall RA, Ostedgaard LS, Premont RT, Blitzer JT, Rahman N, Welsh MJ, Lefkowitz RJ (1998a). A C-terminal motif found in the β_2-adrenergic receptor, P2Y1 receptor and cystic fibrosis transmembrane conductance regulator determines binding to the Na^+/H^+ exchanger regulatory factor family of PDZ proteins. Proc Natl Acad Sci USA 95, 8496–8501.

Hall RA *et al.* (1998b). The β_2-adrenergic receptor interacts with the Na^+/H^+-exchanger regulatory factor to control Na^+/H^+ exchange. Nature 392, 626–630.

Hancock JF (2006). Lipid rafts: contentious only from simplistic standpoints. Nat Rev Mol Cell Biol 7, 456–462.

He J, Bellini M, Inuzuka H, Xu J, Xiong Y, Yang X, Castleberry AM, Hall RA (2006). Proteomic analysis of β_1-adrenergic receptor interactions with PDZ scaffold proteins. J Biol Chem 281, 2820–2827.

Hegener O, Prenner L, Runkel F, Baader SL, Kappler J, Häberlein H (2004). Dynamics of β2-adrenergic receptor-ligand complexes on living cells. Biochemistry 43, 6190–6199.

Hern JA, Baig AH, Mashanov GI, Birdsall B, Corrie JET, Lazareno S, Molloy JE, Birdsall NJM (2010). Formation and dissociation of M1 muscarinic receptor dimers seen by total internal reflection fluorescence imaging of single molecules. Proc Natl Acad Sci USA 107, 2693–2698.

Hernández-Deviez DJ, Martin S, Laval SH, Lo HP, Cooper ST, North KN, Bushby K, Parton RG (2006). Aberrant dysferlin trafficking in cells lacking caveolin or expressing dystrophy mutants of caveolin-3. Hum Mol Gen 15, 129–142.

Huppa JB, Davis MM (2003). T-cell-antigen recognition and the immunological synapse. Nat Rev Immunol 3, 973–983.

Ianoul A, Grant DD, Rouleau Y, Bani-Yaghoub M, Johnston LJ, Pezacki JP (2005). Imaging nanometer domains of β-adrenergic receptor complexes on the surface of cardiac myocytes. Nat Chem Biol 1, 196–202.

Kenworthy AK, Nichols BJ, Remmert CL, Hendrix GM, Kumar M, Zimmerberg J, Lippincott-Schwartz J (2004). Dynamics of putative raft-associated proteins at the cell surface. J Cell Biol 165, 735–746.

Kholodenko BN, Hancock JF, Kolch W (2010). Signalling ballet in space and time. Nat Rev Mol Cell Biol 11, 414–426.

Krupnick JG, Gurevich VV, Schepers T, Hamm HE, Benovic JL (1994). Arrestin-rhodopsin interactions. Multi-site binding delineated by peptide inhibition. J Biol Chem 269, 3226–3232.
Lagerström MC, Schiöth HB (2009). Structural diversity of G protein-coupled receptors and significance for drug discovery. Nat Rev Drug Discovery 7, 339–357.
Lidke DS, Lidke KA, Reiger B, Jovin TM, Arndt-Jovin D (2005). Reaching out for signals: filopodia sense EGF and respond by directed retrograde transport of activated receptors. J Cell Biol 170, 619–626.
Lui G, Shi J, Yang L, Cao L, Park SM, Cui J, Marx SO (2004). Assembly of Ca^{2+}-dependent BK channel signaling complex by binding to β2 adrenergic receptor. EMBO J 23, 2196–2205.
Luttrell LM *et al*. (1999). β-Arrestin dependent formation of β2 adrenergic receptor-Src protein kinase complexes. Science 283, 655–661.
Malbon CC, Tao J, Wang H-Y (2004). AKAPs (A-kinase anchoring proteins) and molecules that compose their G-protein-coupled receptor signalling complexes. Biochem J 379, 1–9.
Mukherjee S, Palczewski K, Gurevich VV, Hunzicker-Dunn M (1999). β-Arrestin-dependent desensitization of lutenizing hormone/choriogonadotropin receptor is prevented by a synthetic peptide corresponding to the third intracellular loop of the receptor. J Biol Chem 274, 12984–12989.
Murakoshi H, Iino R, Kobayahi T, Ohshima C, Yoshimura A, Kusumi A (2004). Single-molecule imaging analysis of Ras activation in living cells. Proc Natl Acad Sci USA 101, 7317–7322.
Naren AP *et al*. (2003). A macromolecular complex of β_2 adrenergic receptor, CFTR and ezrin/radixin/moesin-binding phosphoprotein 50 is regulated by PKA. Proc Natl Acad Sci USA 100, 342–346.
Nauert JB, Klauck TM, Langeberg LK, Scott JD (1997). Gravin, and autoantigen recognized by serum from myasthenia gravis patients, is a kinase scaffold protein. Curr Biol 7, 52–62.
Negro A, Dodge-Kafka K, Kapiloff MS (2008). Signalosomes as therapeutic targets. Prog Pediatr Cardiol 25, 51–56.
Oliveria SF, Gomez LL, Dell'Acqua ML (2003). Imaging kinase–AKAP79–phosphatase scaffold complexes at the plasma membrane in living cells using FRET microscopy. J Cell Biol 160, 101–112.
Parton RG, Simons K (2007). The multiple faces of caveolae. Nat Rev Mol Cell Biol 8, 185–194.
Pelkmans L, Zerial M (2005). Kinase-regulated quantal assemblies and kiss-and-run recycling of caveolae. Nature 436, 128–133.
Pierce KL, Premont RT, Lefkowitz RJ (2002). Seven-transmembrane receptors. Nat Rev Mol Cell Biol 3, 639–650.
Pieretti F, Depez-Beauclair P, Bonardo B, Aubert H, Juhan-Vague I, Nalbone G (2003). Identification of SAP97 as an intracellular binding partner of TACE. J Cell Sci 116, 1949–1957.
Pontier SM, Percherancier Y, Galadrin S, Breit A, Galés C, Bouvier M (2008). Cholesterol-dependent separation of the β2-adrenergic receptor from its partners determines signaling efficacy. J Biol Chem 283, 24659–24672.
Rockman HA, Koch WJ, Lefkowitz RJ (2002). Seven-transmembrane-spanning receptors and heart function. Nature 415, 206–212.
Ruehr ML, Russell MA, Bond M (2004). A-kinase anchoring protein targeting of protein kinase A in the heart. J Mol Cell Cardiol 37, 653–665.
Rybin VO, Xu X, Lisanti MP, Steinberg SF (2000). Differential targeting of β-adrenergic receptor subtypes and adenylyl cyclase to cardiomyocyte caveolae. A mechanism to functionally regulate the cAMP signaling pathway. J Biol Chem 275, 41447–41457.
Sergé A, Fourgeaud L, Hémar A, Choquet D (2002). Receptor activation and Homer differentially control the lateral mobility of metabotropic glutamate receptor 5 in the neuronal membrane. J Neurosci 22, 3910–3920.
Shcherbakova OG, Hurt CM, Xiang Y, Dell'Acqua ML, Zhang Q, Tsien RW, Kobilka BK (2007). Organization of β-adrenoceptor signaling compartments by sympathetic innervation of cardiac myocytes. J Cell Biol 176, 521–533.
Song KS, Tang Z, Li S, Lisanti MP (1997). Mutational analysis of the properties of caveolin-1. A novel role for the C-terminal domain in mediating homo-typic caveolin-caveolin interactions. J Biol Chem 272, 4398–4403.
Steinberg SF (2004). β2-Adrenergic receptor signaling complexes in cardiomyocyte caveolae/lipid rafts. J Mol Cell Cardiol 37, 407–415.
Suzuki K, Ritchie K, Kajikawa E, Fujiwara T, Kusumi A (2005). Rapid hop diffusion of a G-protein-coupled receptor in the plasma membrane as revealed by single-molecule techniques. Biophys J 88, 3659–3680.
Tang Y, Hu LA, Miller WE, Ringstad N, Hall RA, Pitcher JA, DeCamilli P, Lefkowitz RJ (1999). Identification of the endophilins (SH3p4/p8/p13) as novel binding partners for the β1-adrenergic receptor. Proc Natl Acad Sci USA 96, 12559–12564.
Tao J, Wang H-Y, Malbon CC (2003). Protein kinase A regulates AKAP250 (gravin) scaffold binding to the $_2$-adrenergic receptor. EMBO J 22, 6419–6429.
Wong W, Scott JD (2004). AKAP signaling complexes: focal points in space and time. Nat Rev Mol Cell Biol 5, 959–970.
Wu H, Reuver SM, Kuhlendahl S, Chung WJ, Garner CC (1998). Subcellular targeting and cytoskeletal attachment of SAP97 to the epithelial lateral membrane. J Cell Sci 111, 2365–2378.
Xiang Y, Devic E, Kobilka BK (2002a). The PDZ binding motif of the β_1-adrenergic receptor modulates receptor trafficking and signaling in cardiac myocytes. J Biol Chem 277, 33783–33790.
Xiang Y, Kobilka BK (2003). Myocyte adrenoceptor signaling pathways. Science 300, 1530–1532.
Xiang Y, Rybin VO, Steinberg SF, Kobilka BK (2002b). Caveolar localization dictates physiologic signaling of β_2-adenoreceptors in neonatal cardiac myocyte. J Biol Chem 277, 34280–34286.
Xiao RP, Zhu W, Zheng M, Cao C, Zhang Y, Lakatta EG, Han Q (2006). Subtype-specific α_1- and β-adrenoceptor signaling in the heart. Trends Pharmacol Sci 27, 330–337.
Yan X, Walkiewicz M, Carlson J, Leiphon L, Grove B (2009). Gravin dynamics regulates the subcellular distribution of PKA. Exp Cell Res 315, 1247–1259.
Yudowski GA, Puthenveedu MA, von Zastrow M (2006). Distinct modes of regulated receptor insertion to the somatodendritic plasma membrane. Nat Neurosci 9, 622–627.
Zaccolo M, Magalhães P, Pozzan T (2002). Compartmentalization of cAMP and Ca^{2+} signals. Curr Opin Cell Biol 14, 160–166.
Zeke A, Lukacs M, Lim WA, Remenyi A (2009). Scaffolds: interaction platforms for cellular signalling circuits. Trends Cell Biol 19, 364–374.
Zheng C-Y, Petralia RS, Wang Y-X, Kacher B, Wenthold RJ (2010). SAP102 is a highly mobile MAGUK in spines. J Neurosci 30, 4757–4766.
Zheng M, Zhu W, Han Q, Xiao R-P (2005). Emerging concepts and therapeutic implications of β-adrenergic receptor subtype signaling. Pharmacol Ther 108, 257–268.
Zhong H, Sia G-M, Sato TR, Gray NW, Mao T, Khuchua Z, Huganir RL, Svoboda KL (2009). Subcellular dynamics of type II PKA in neurons. Neuron 62, 363–374.